frontiers | Frontiers in Astronomy and Space Sciences

TYPE Original Research
PUBLISHED 06 June 2023
DOI 10.3389/fspas.2023.1213294

OPEN ACCESS

EDITED BY
Bojing Zhu,
Chinese Academy of Sciences (CAS), China

REVIEWED BY
Lianghai Xie,
Chinese Academy of Sciences (CAS), China
Hong Jin,
Chinese Academy of Sciences (CAS), China
Xiaoping Zhang,
Macau University of Science and Technology, Macao SAR, China
Lifang Li,
Harbin Institute of Technology, China
Jianhong Zhuang,
China Academy of Space Technology, China
Chengxuan Zhao,
China Academy of Space Technology, China

*CORRESPONDENCE
Hong Gan,
ganhong06@gmail.com
Guangfei Wei,
gfwei0554@gmail.com

RECEIVED 27 April 2023
ACCEPTED 24 May 2023
PUBLISHED 06 June 2023

CITATION
Gan H, Wei G, Zhang X, Xia G and Shi J (2023), Experimental study on electrostatic migration of different mineral particles composing lunar dust under electron irradiation.
Front. Astron. Space Sci. 10:1213294.
doi: 10.3389/fspas.2023.1213294

Experimental study on electrostatic migration of different mineral particles composing lunar dust under electron irradiation

Hong Gan[1]*, Guangfei Wei[1,2]*, Xiao Zhang[1,3], Guojun Xia[1,3] and Jingjing Shi[1]

[1]Deep Space Exploration Laboratory, Hefei, China, [2]Center for Excellence in Comparative Planetology, Chinese Academy of Sciences, Hefei, China, [3]Shanghai Institute of Satellite Engineering, Shanghai, China

Dust electrostatic migration is one of the primary causes of dust events on the surface of airless celestial bodies, which can result in multiple dust phenomena, including lunar horizon glow and dust pools, and also offer crucial insights into the evolution of the surface materials of airless celestial bodies. To date, the characteristics and laws of dust electrostatic migration are still not well understood. Here, we report the electrostatic migration characteristics of pyroxene, olivine, and ilmenite particles measured by the laser Doppler method and compare them with the findings of anorthite particles in previous experiments to recognize the differential migration characteristics of different mineral components in the lunar dust. The results demonstrate that the particle sizes of most moving pyroxene and olivine particles are in the range of 0–10 μm, and their vertical velocities are typically less than 2 m s^{-1}, which are consistent with the previous studies. The cohesive force between the dust particles is probably what causes the difference in the migration rates of various insulating minerals. Note that no moving ilmenite particles were detected probably due to the material's good conductivity. It can be speculated that the concentration of fugitive dust in the lunar mare is affected by the ilmenite content, but further research is needed to determine how low ilmenite content can cause dust migration.

KEYWORDS

lunar surface, lunar dust, mineral particles, electron irradiation, electrostatic migration

1 Introduction

In the 1960s, the lunar horizon glow was observed several times by the Surveyor 5, 6, and 7 missions (Criswell, 1973; Rennilson and Criswell, 1974; Colwell et al., 2007). This is the earliest space phenomenon that may be related to electrostatic dust migration. Subsequently, the astronauts of Apollo 17 described high-altitude lunar horizon glow that was visible above the lunar surface (McCoy, 1976; Zook and McCoy, 1991). Recently, five dust enhancement events during the Lunar Atmosphere and Dust Environment Explorer mission were recognized (Xie et al., 2020), which provides concrete evidence of electrostatic dust migration above the lunar surface. This phenomenon was also confirmed by the dust

deposition phenomenon at a height of 190 cm above the surface of the Chang' E-3 landing site (Li et al., 2019; Zhang et al., 2020) and the reflectance feature difference of lunar rocks and regolith observed by the Chang' E-3 mission due to long-term dust activity (Yan et al., 2019).

Meanwhile, lunar dust is a very important space environmental factor on the lunar surface. The electrostatic levitation or migration of lunar dust will cause potential hazards to spacecraft and engineering systems (Gaier and Jaworske, 2007; Kawamoto et al., 2011; Zakharov et al., 2020), such as the malfunction of seals for on/off mechanisms or space suits and the functional degradation of the heat rejection systems. It is closely related to the achievement of space exploration scientific goals and even the success or failure of the entire exploration mission. Therefore, the study of the charging and migration mechanism of lunar dust in the lunar space environment not only provides scientific support for the research on the causes of the lunar horizon glow observed during the Surveyor and Apollo missions, but also provides theoretical guidance for the design of lunar dust removal strategies on optics, mechanisms, and human space flight hardware in subsequent lunar exploration missions.

In the last two decades, a series of experiments have been carried out to study the causes, conditions, and characteristics underlying the migration behavior of dust particles. The interaction of electrons and dust particles was believed to play an important role in dust charging and migration. For the individual micron-/submicron-size dust particles, the charging characteristics of dust particles from Apollo 11 and 17 dust samples (0.2–13 μm) (Abbas et al., 2010) and Lunar Highlands Type regolith simulants (0.3–3 μm) (Němeček et al., 2011) were measured under electron irradiation. The results showed that the secondary emission yield increases with the primary beam energy, reaching a maximum of approximately 3 at 350 eV, and the surface potentials are independent of the grain mass, shape, and dimensions for the grains with sizes between 0.3 and 3 μm and electron energies lower than 200 eV (Němeček et al., 2011), while for larger particles, the surface potentials of dust grains are a function of the particle size, electron energy, and electron flux density (Abbas et al., 2010). The results could be used to explain the charging of the isolated suspended dust particle. However, the lunar dust layer is accumulated by the countless dust particles. There are substantial differences between the charging and migration characteristics of individual small-size dust grains and the corresponding bulk materials. Lunar Prospector measurements of surface potentials and electron fluxes from the lunar regolith suggest that the secondary electron yield from lunar regolith is close to 1.0–1.1 (Halekas et al., 2009a), which is about three times smaller than the yield in the previous studies. This is consistent with the observation that the lunar surface potential usually remains negative in the shadow regions under various solar wind conditions (Halekas et al., 2009b).

It has been proved that dust particles can be released from the bulk samples and then migrate under electron irradiation (Wang et al., 2010). The particle size, vertical velocity, transport rate, and launch angle distribution of lofted dust particles were experimentally studied. The results showed that the diameters of most dust particles are below 10 μm and the verticle velocities are constrained by diameters (Carroll et al., 2020; Gan et al., 2022). The micron-sized insulating dust particles jump to centimetres or tens of centimetres in height with an initial speed below approximately 2 m s^{-1} exposure to electron irradiation with or without plasmas, resulting in an equivalent height below approximately **1** m on the lunar surface (Wang et al., 2016; Örger et al., 2019; Gan et al., 2022). The height is comparable to that of the so-called lunar horizon glow. The transport rate is a function of time (Hood et al., 2018; Gan et al., 2022). Based on the experimental results, the patched charge model was proposed to explain that the intense particle-particle repulsive forces are due to the re-absorption of secondary electrons at the walls of microcavities formed between neighboring dust particles (Wang et al., 2016; Schwan et al., 2017). This means that the net charge of dust particles lofted on the surfaces of airless planetary bodies is negative. Due to the increased packing density, the contact area between particles increases and the dust activity weakens, since the packing density is related to the number and size of the microcavities (Örger et al., 2019). In addition, most particles were launched from the sample surface in a direction closer to the surface normal. However, the peak value of the launch angles is around 43.5°–45° from the surface normal, and the launching angle distribution of dust particles in two horizontal directions (both ± x-axis) is quite similar (Örger et al., 2021).

Lunar dust is made of fine minerals, glass, and debris on the lunar surface. The charging properties and migration characteristics of each component of lunar dust are very different, but have not been comprehensively studied. Previous studies focused on the migration characteristics of lunar dust samples (mixture), lunar dust simulants (mixture), and silica dust. The results are not conducive to explaining the differences in migration characteristics of each component. Therefore, based on the previous measurements of the electrostatic migration characteristics of anorthite particles (Gan et al., 2022), here we present the laboratory results on the electrostatic migration characteristics of pyroxene, olivine, and ilmenite particles. The differences in the electrostatic migration characteristics of each component are compared to confirm the main influencing factors.

2 Experimental setup

The Lunar (Planetary) Dust Environment Simulation Platform, as shown in **Figure 1**, utilizes a spherical stainless-steel vacuum chamber for conducting experiments. The platform was designed to experimentally simulate the migration process of charged dust particles, and then the influence of dust components on its charging and transport characteristics will be discussed. The main testing chamber is 50 cm in diameter and has a base pressure of 10^{-6} Pa. On the chamber's ceiling, an electron gun is mounted and electrons are injected into the sample surface at a 45° angle. The energies of electrons (E_0) range from 0 to 500 eV and the emission currents (I_0) range from 1 to 500 μA. The incident electrons are denser and more energetic than the typical solar wind, which can represent the condition parameters in the special plasma environment, such as in the lunar crater wake, plasma sheet, and magnetosheath regions, as well as during the solar energetic particle (SEP) events. While the current is dramatically enhanced to obtain a larger dust flux.

Under electron irradiation, dust particles are charged and released from the surface. Phase Doppler Particle Analyzer (PDPA)/Laser Doppler Velocimeter (LDV) system from TSI Incorporated (Saint Paul, MN 55126, United States,

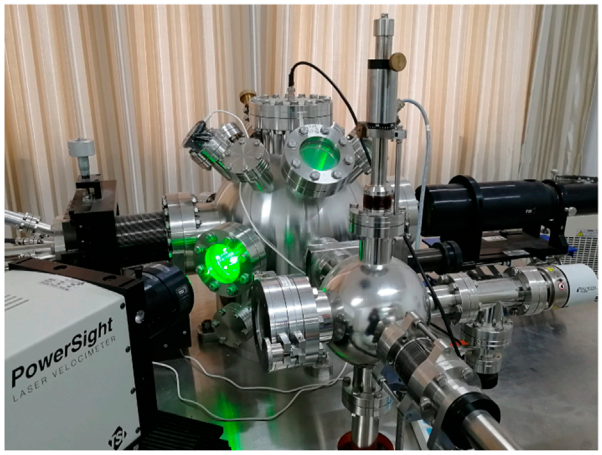

FIGURE 1
Pictorial view of the lunar (Planetary) dust environment simulation platform.

https://www.tsi.com/products/fluid-mechanics-systems/) has been employed to detect the moving dust particles. The intersection of two laser beams creates a series of light and dark fringes. Since the moving particles scatter light when crossing the bright fringe but scatter no light when passing the dark fringe, a fluctuating pattern of scattered light intensity with a frequency (f_D) is generated. The velocities of moving particles (V) can be calculated by multiplying the frequency by the known fringe spacing (δ_f):

$$V = \delta_f \cdot f_D, \tag{1}$$

where δ_f is determined by the laser wavelength (λ) and the angle (2κ) between beams:

$$\delta_f = \frac{\lambda}{2\sin(\kappa)}. \tag{2}$$

The particle diameter (D) can be obtained by the phase Doppler technique, which is an extension of LDV, allowing the size measurements of spherical particles to be obtained. The spatial frequency (spacing between the scattered fringes at the light collecting optics) of the scattered fringes can be measured as a phase shift (Φ) between two electrical signals resulting from the scattered light. The diameter is correlated to the phase shift between two laser beams from two corresponding detectors at different positions:

$$D = \frac{L_f \delta_f \Phi}{2\pi \Delta l} K, \tag{3}$$

where K is the optical constant, Δl is the space between two detectors, and L_f is the lens focal length. The detectable diameters of the moving dust particles are between 0.5 and 90 μm and velocities are between −90 and 283 m s^{-1}.

In this work, we first crushed and sieved the pyroxene and olivine samples from Damaping, Hebei Province, China and the ilmenite sample from Panzhihua, Sichuan Province, China. Second, the dust particles with diameters smaller than 40 μm were loosely placed in a square stainless-steel box (8 mm wide and 1 mm deep) for testing. The mean particle sizes of pyroxene, olivine, and ilmenite particles are 10.46, 11.48, and 4.57 μm, respectively. An insulating plate is placed between the sample box and the grounded sample stage, and the sample box is directly connected to a voltmeter. The beam spot of incident electrons was adjusted to 10 mm to prevent the electron beam impact/shadow boundaries from affecting particle transport (Wang et al., 2011). Third, before the electron beam incident, the pyroxene particles were baked at 110°C for 24 h in atmospheric conditions and deaerated for 12 h in a vacuum chamber with a pressure of 10^{-6} Pa to eliminate adsorbed gases.

Finally, under electron irradiation, the dust particles obtain charges that can be maintained for a long time. After overcoming the gravity and cohesive force, the dust particles migrate. The diameters and velocities of the moving dust particles were measured by PDPA/LDV under different electron irradiation conditions. Note that the height of the measured point (h_0), which refers to the distance between the sample surface and the measured point, was set to 4 mm here, which can be adjusted by moving the sample stage vertically.

3 Experimental results

PDPA/LDV system did not detect the moving ilmenite particles. However, both pyroxene and olivine particles had massive electrostatic migration and showed similar movement characteristics. Here, we take the electrostatic migration of pyroxene particles as an example to elaborate on its motion characteristics.

3.1 Diameter and velocity characteristics of moving pyroxene particles

We recorded 19 groups of experimental results on pyroxene migration, including the dust migration characteristics under the incident electron beam with different energies and currents. Though each experiment only lasted approximately 3–7 min, up to more than 10,000 particles were detected. However, most of the particle size and vertical velocity are still in the range of 0–10 μm and 0–2 m s^{-1}, respectively, similar to the migration characteristics of anorthite particles (Gan et al., 2022). **Figure 2**, for example, presents the migration characteristics of pyroxene particles under electron irradiation with an energy of 350 eV and a current of 500 μA, including the distributions of diameters (**Figure 2A**) and vertical velocities (**Figure 2B**), and the relationship of diameters and vertical velocities (**Figure 2C**). The red line in **Figures 2A, B** represents the cumulative particle counts. The electron beam was continuously injected for 411 s. A total of 7,760 diameter signals and 11,517 vertical velocity signals were recorded. There are 7,605 moving particles with a diameter below 10 μm (accounting for 98%), while 6,769 particles smaller than 5 μm (accounting for 87%). The moving particles with velocities in the 0–2 m s^{-1} and 0–1 m s^{-1} ranges consist of 11,447 and 10,071 particles, respectively, accounting for 99% and 87% of the total. Note that during the first few seconds, the moving dust particles increased significantly due to the extremely loose top surface layer. This layer was either the topmost layer of the bulk sample or was formed by the sedimentation of moving particles in the previous set of experiments. **Figure 2C** indicates that the vertical velocities of the moving particles are constrained by the

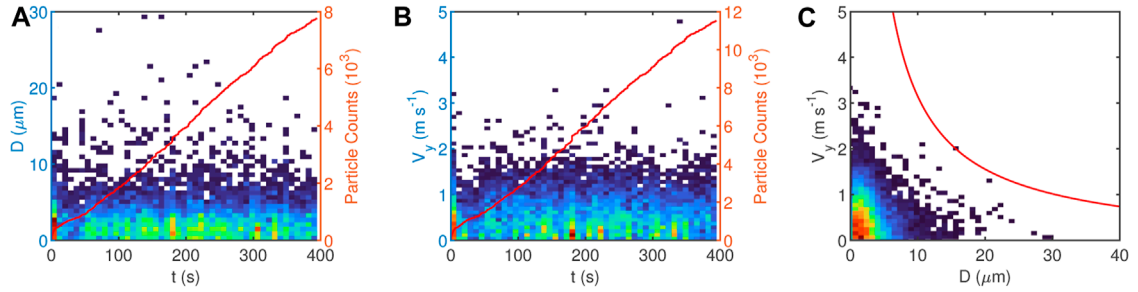

FIGURE 2
Distributions of diameters **(A)** and vertical velocities **(B)**, and the relationship between diameters and vertical velocities **(C)**. The red lines in **(A)** and **(B)** represent cumulative counts of particle size and velocity signals of moving pyroxene particles, and the red line in **(C)** is the envelope curve based on the constraint relation between vertical velocity and particle size.

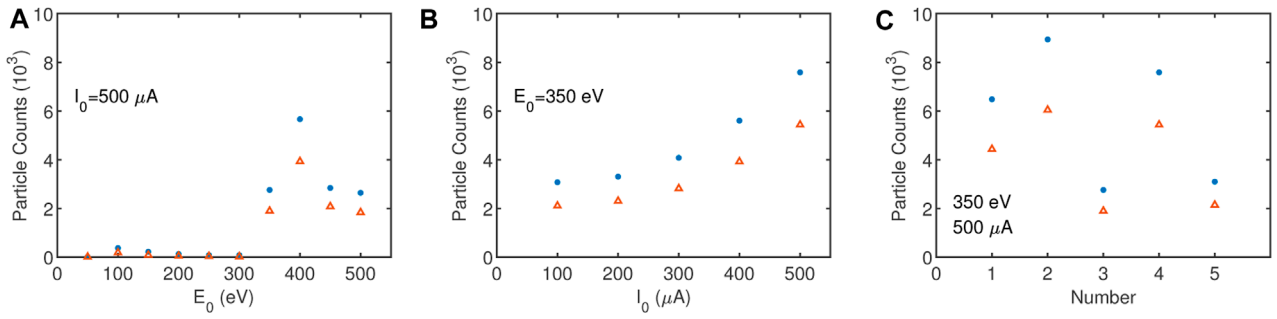

FIGURE 3
Relationships of dust counts with the electron energy **(A)** and electron current **(B)**. **(C)** shows the results of multiple parallel experiments under electron irradiation with the same energy and current conditions. The blue dot and the red triangle indicate the signal counts of vertical velocities and diameters of the moving particles, respectively.

particle size. The red envelope curve is given based on the energy conservation law.

3.2 Influencing factor of pyroxene migration characteristics

To analyze the main factors affecting the motion characteristics of pyroxene particles, Figure 3 presents the relationships of dust counts with the electron energy (a) and current (b), as well as the results (c) of multiple parallel experiments under electron irradiation with an energy of 350 eV and a current of 500 μA. Particle counts are the number of moving particles within the first 5 min of each experiment, excluding the first few seconds when the dust flux increases significantly. Figure 3A shows that the number of moving pyroxene particles changes with an energy of incident electrons when the current of incident electrons was 500 μA. As shown in Figure 3A, when the energy of incident electrons is less than 300 eV, the total number of lofted pyroxene particles is less than 400 (based on the verticle velocity signals), while the total number of pyroxene particles is more than 2,500 (based on the verticle velocity signals) when the electron energy is higher than 350 eV. This means the total number of the moving pyroxene particles has a dividing line at the electron energy of 300–350 eV. The reason may be that the secondary electron yield of pyroxene particles varies with an energy of the incident electrons, which leads to a change in its charging characteristics and surface potential distribution.

Figure 3B shows that the number of moving pyroxene particles varies with the current of incident electrons when the electron energy was set to 350 eV. It can be found that the number of pyroxene particles is always higher than 3,000 (based on the verticle velocity signals) for the incident electron current in the range of 100–500 μA, and the number increases as the electron current increases. Furthermore, we consider the variation in the number of moving pyroxene particles with depth under certain electron energy and current conditions. Therefore, multiple experiments under electron irradiation with an energy of 350 eV and a current of 500 μA were interspersed throughout the experiments, as shown in Figure 3C. The number of moving pyroxene particles is between 2,700 and 9,000. The possible reason for the large variation range of dust counts is the uneven density of dust accumulation. For naturally loose dust with a thickness below 1 mm, the local stacking density is not uniform. As the rising dust phenomenon continues to occur, the dust on the top surface and then the subsurface is stripped in succession. With the increase in depth, the local packing density varies randomly, resulting in a significant influence of the local porosity or compactness on the amount of lofted dust particles.

4 Discussions

The migration rate is defined here as the number of migrating particles per second to further analyze the migration characteristics of the moving pyroxene, olivine, and ilmenite particles. We compare our results with the previous studies on the anorthite transport rates derived from (Gan et al., 2022). **Figure 4** presents the migration rates of anorthite (An), olivine (Ol), pyroxene (Py), and ilmenite (Ilm) particles under electron irradiation with an energy of 350 eV and a current of 500 μA. Note that the height of the measured point is 6 mm in the anorthite migration experiments, while the height is 4 mm in the migration experiments of three other minerals. Based on the height difference of only 2 mm between the two measured points, we assume that there is no dramatic variation in the migration fluxes of the identical mineral particles at observed heights above. A qualitative comparison study is therefore effective. The results show that the transport rates of olivine and pyroxene particles are in the range of 6–21 and 9–30 particles per second, higher than the rates of anorthite particles (0.1–2 particles per second). The rate of ilmenite particles is zero. The above results demonstrate that there is a significant difference in the electrostatic transport characteristics of different minerals in the lunar dust.

Ilmenite is a titanium-iron oxide mineral with weak magnetism and good conductivity, while anorthite, olivine, and pyroxene are insulating silicate minerals. Due to the weak magnetism of ilmenite particles, some low-energy incident electrons are deflected or returned, so that the incident electron current slightly decreases in varying degrees. What's more, due to the good conductivity of ilmenite particles, the charge on the particle surface was transferred, resulting in the lack of charge accumulation. Therefore, ilmenite particles could not be released from the sample surface, which is consistent with our experimental findings that no ilmenite particles were detected. Whereas, the charge accumulated by the insulating silicate mineral particles, such as anorthite, olivine, and pyroxene, is difficult to transfer, which caused the dust movement to occur when the three insulating mineral particles were exposed to electron irradiation.

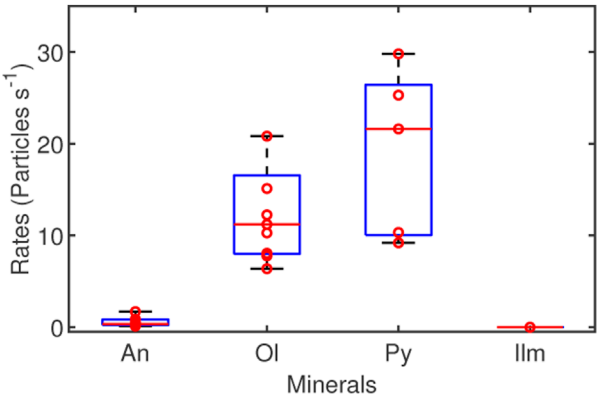

FIGURE 4
Transport rates of anorthite (An), olivine (Ol), pyroxene (Py), and ilmenite (Ilm) particles. Note that the height of the measured point is 4 mm for all experiments, except anorthite migration experiments (6 mm).

It can be concluded that the difference in electrostatic migration characteristics of different minerals is closely related to their electrical properties, such as conductivity or permittivity. Assuming that the lunar dust in different regions is composed of four minerals mixed in different proportions. For example, a small amount of ilmenite particles is dispersed in a large amount of insulating silicate mineral particles, so that the ilmenite particles cannot contact each other. In this case, the ilmenite particles may also migrate. The effect of the different percentages of ilmenite particles on lunar dust migration will be further investigated to understand the dust migration characteristic differences between the highlands and the maria, including the migration characteristic differences between the regions with high-Ti and low-Ti basalts. The results can also be inferred that low-titanium lunar soil may be more prone to migration than high-titanium lunar soil. It is worth noting that the proportion of the four kinds of mineral particles changes as the differential migration of each mineral dust. When the dust migration stops may depend on the percentage of ilmenite particles in the lunar soil.

The migration rates of three insulating silicate minerals are also different, possibly due to the distinct chemical compositions, crystal structures, and physical properties. Anorthite, olivine, and pyroxene are framework silicate, nesosilicate, and chain silicate minerals, respectively. Permittivity refers to a substance's ability to retain an electric charge. However, their permittivities are similar and range from 6.5 to 8. Density and diameter determine the magnitude of gravity that a particle has to overcome to leave the sample surface. In theory, anorthite is easier to migrate because of its lower density. However, in practice, it has the lowest migration rate compared to other silicate minerals. This may be attributed to the stronger cohesive force and higher measuring point. In particular, the effect of the cohesive force on dust migration rate is one of the key contents of subsequent work.

For large dust particles with a diameter of tens of microns, it is mainly the gravity force that needs to be overcome during the process of dust particles being released, while the cohesive force needs to be overcome for micron-sized dust particles (Hartzell and Scheeres, 2011). The cohesive force is mainly derived from the contribution of electrostatic force and van der Waals force related to surface energy. That is, the cohesive force depends on the contact area, effective surface energy, etc. The contact area is related to the distance between particles (namely, packing density), particle size, and particle shape. To exclude the influence of the particle size and shape on dust transport rate, the particle size distributions and shape characteristics of olivine, pyroxene, and ilmenite are further presented, as shown in **Figures 5**, **6**, respectively. Both olivine and pyroxene particles were directly ground in the mortar, and have similar particle size distribution characteristics (below 40 μm). Due to the higher hardness of ilmenite particles, the wet grinding method with alcohol was used. This method is more effective, and the particle size of ilmenite particles is concentrated below 20 μm. In addition, the grain shapes of olivine, pyroxene, and ilmenite minerals are angular. This means that the particle size and shape are not the main reasons for the difference in the transport rates of olivine and pyroxene particles.

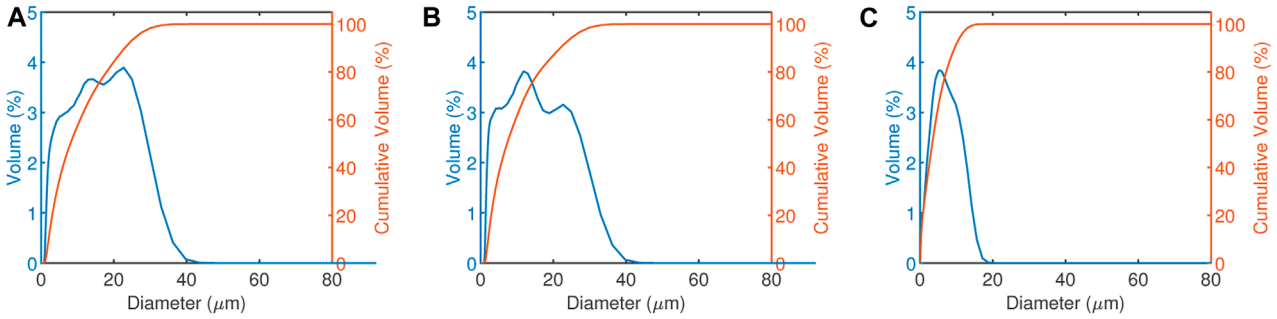

FIGURE 5
The blue lines represent the particle size distributions of olivine **(A)**, pyroxene **(B)**, and ilmenite **(C)** particles, and the red lines represent the accumulative volume of three mineral particles (unit: vol%).

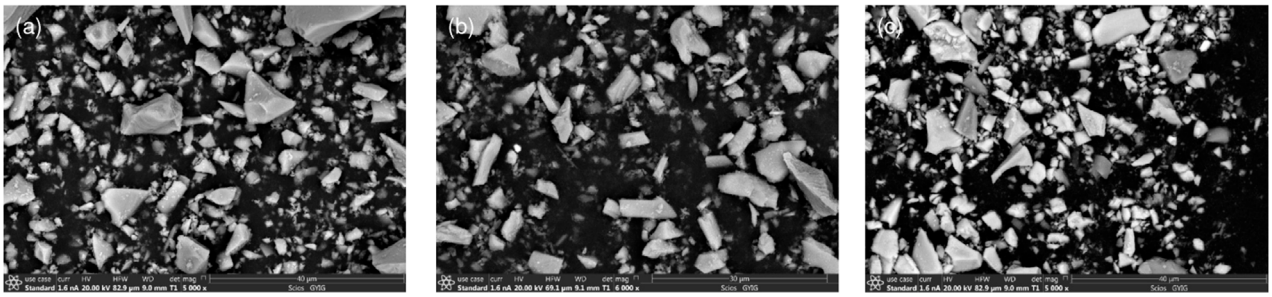

FIGURE 6
Shape characteristics of olivine **(A)**, pyroxene **(B)**, and ilmenite **(C)** particles.

Undoubtedly, the packing density is a major influencing factor. Figure 3C has demonstrated that the influence of the porosity or compactness on dust migration is prominent. However, it is speculated that the difference in the transport rate ranges between olivine and pyroxene may be caused by the difference in the surface energy, since the surface energy depends on the composition of dust particles. Moreover, in the hard vacuum conditions of the lunar environment, the effective surface energy is up to two orders of magnitude greater than that in humid air at one atmosphere pressure (Walton, 2007). Especially for fine lunar dust, the surface energy per unit mass available for cohesive forces to act in the bulk material increases as the surface area per unit mass increases, which is also the reason for the strong adhesion of fine lunar dust.

It should be emphasized that the composition of the lunar dust is much more complex than that of the experimental sample. Lunar dust is the fine fraction of lunar soil. Due to the long-term interaction of lunar soil with the space environment, lunar soil is composed of various types of particles, including rock fragments, mono-mineralic fragments, various kinds of glasses, and agglutinates. The lithic fragments always feather ultrathin amorphous coatings and nanophase iron residing in them. Agglutinates are aggregates of crystalline grains and lithic fragments bonded together by glass. The changes in material composition and crystal structure caused by space weathering can alter the effective surface energy of dust particles. This means the electrostatic migration and adhesion of dust on the lunar surface are more complicated.

5 Conclusion

To analyze the influence of lunar dust composition on the characteristics of dust electrostatic migration, we focus on the simulation of the electrostatic migration processes of pyroxene, olivine, and ilmenite. The results demonstrate that pyroxene and olivine particles can migrate, while ilmenite particles can not. The moving pyroxene and olivine particles are statistically smaller than 10 μm in size, and their verticle velocities are typically less than 2 m s^{-1}, which are consistent with the migration characteristics of anorthite particles in the previous studies. The verticle velocities are also constrained by the particle size.

The particle counts at the measured point vary with the energy and a current of incident electrons, as well as the packing density of dust particles. The energy threshold of massive dust migration is between 300 and 350 eV. The number of migrating dust particles is fewer than 400 within 5 min when the energy of the incident electron is less than 300 eV and the current is 500 μA. However, when the energy of the incident electron is higher than 350 eV, the number is higher than 2,500. The particle counts increase with the increase in the electron current. The dust particles accumulate loosely, and the local stacking density in the

loose dust layer is unpredictable, so that the counts of the moving particles do not follow the law of monotonous change. It can be seen from the parallel experiments of pyroxene migration process simulations under electron irradiation with an energy of 350 eV and a current of 500 μA, the migration rates are between 9 and 30 particles per second due to the different stacking compactness. On the lunar surface, lunar regolith continues to churn under meteorite/micrometeorite bombardment, forming an extremely loose lunar soil layer, which will considerably facilitate lunar dust migration.

Meanwhile, to confirm that the material composition affects dust migration characteristics, we compared the migration rates of anorthite, olivine, pyroxene, and ilmenite particles at the measured point. As mentioned above, insulating silicate minerals like anorthite, olivine, and pyroxene are more likely to migrate than ilmenite particles with stronger conductivity. Secondly, the cohesive force may have a sizable impact on dust migration. Pyroxene and olivine particles, for example, have comparable densities, particle sizes, shapes, and dielectric constants. The difference in migration characteristics may be mostly caused by the cohesive force associated with the surface energy, packing density, and other factors. Further analysis of the influence of packing density of lunar dust on its electrostatic migration rate can offer scientific guidance for dust mitigation in the future lunar surface exploration and lunar base construction, such as whether the lunar dust can be by merely tamping the lunar soil rather than consolidating it through microwave sintering.

Data availability statement

The raw data supporting the conclusion of this article will be made available by the authors, without undue reservation.

Author contributions

HG was involved in the experimental design, experimental testing, data analysis, and manuscript writing and revision. GW supervised the experimental design and the writing of the manuscript and participated in the revision of the manuscript. XZ, GX, and JS contributed to the manuscript's writing and revision. All authors contributed to the article and approved the submitted version.

Funding

This research was funded by the National Key Research and Development Program of China (2022YFF0711400), the National Natural Science Foundation of China (42241154 and 41903058), the Frontier Science Research Program of Deep Space Exploration Laboratory (2022-QYKYJH-HXYF-023), and the Science and Technology Program of Guizhou Province (QKHJC-ZK[2023]-131 and QKHJC-ZK[2023]-476).

Acknowledgments

The authors thank the Center for Lunar and Planetary Sciences, Institute of Geochemistry, Chinese Academy of Sciences for providing testing services.

Conflict of interest

The authors declare that the research was conducted in the absence of any commercial or financial relationships that could be construed as a potential conflict of interest.

Publisher's note

Supplementary material

The Supplementary Material for this article can be found online at: https://www.frontiersin.org/articles/10.3389/fspas.2023.1213294/full#supplementary-material

References

Abbas, M., Tankosic, D., Craven, P., LeClair, A., and Spann, J. (2010). Lunar dust grain charging by electron impact: Complex role of secondary electron emissions in space environments. *Astrophysical J.* 718, 795–809. doi:10.1088/0004-637x/718/2/795

Carroll, A., Hood, N., Mike, R., Wang, X., Hsu, H.-W., and Horányi, M. (2020). Laboratory measurements of initial launch velocities of electrostatically lofted dust on airless planetary bodies. *Icarus* 352, 113972. doi:10.1016/j.icarus.2020.113972

Colwell, J., Batiste, S., Horányi, M., Robertson, S., and Sture, S. (2007). Lunar surface: Dust dynamics and regolith mechanics. *Rev. Geophys.* 45. doi:10.1029/2005rg000184

Criswell, D. R. (1973). "Horizon-glow and the motion of lunar dust," in *Photon and particle interactions with surfaces in space: Proceedings of the 6th eslab symposium, held at noordwijk, The Netherlands, 26–29 september, 1972* (Springer), 545–556.

Gaier, J. R., and Jaworske, D. A. (2007). "Lunar dust on heat rejection system surfaces: Problems and prospects," in *AIP conference proceedings* (American Institute of Physics), 880, 27–34.

Gan, H., Zhang, X., Li, X., Jin, H., Xie, L., and Zou, Y. (2022). Experiments on the electrostatic transport of charged anorthite particles under electron beam irradiation. *Astrophysical J.* 930, 42. doi:10.3847/1538-4357/ac5d48

Halekas, J., Delory, G., Lin, R., Stubbs, T., and Farrell, W. (2009a). Lunar prospector measurements of secondary electron emission from lunar regolith. *Planet. Space Sci.* 57, 78–82. doi:10.1016/j.pss.2008.11.009

Halekas, J., Delory, G., Lin, R., Stubbs, T., and Farrell, W. (2009b). Lunar surface charging during solar energetic particle events: Measurement and prediction. *J. Geophys. Res. Space Phys.* 114. doi:10.1029/2009ja014113

Hartzell, C. M., and Scheeres, D. J. (2011). The role of cohesive forces in particle launching on the moon and asteroids. *Planet. Space Sci.* 59, 1758–1768. doi:10.1016/j.pss.2011.04.017

Hood, N., Carroll, A., Mike, R., Wang, X., Schwan, J., Hsu, H.-W., et al. (2018). Laboratory investigation of rate of electrostatic dust lofting over time on airless planetary bodies. *Geophys. Res. Lett.* 45, 13–206. doi:10.1029/2018gl080527

Kawamoto, H., Uchiyama, M., Cooper, B., and McKay, D. (2011). Mitigation of lunar dust on solar panels and optical elements utilizing electrostatic traveling-wave. *J. Electrost.* 69, 370–379. doi:10.1016/j.elstat.2011.04.016

Li, D., Wang, Y., Zhang, H., Zhuang, J., Wang, X., Wang, Y., et al. (2019). *In situ* measurements of lunar dust at the chang'e-3 landing site in the northern mare imbrium. *J. Geophys. Res. Planets* 124, 2168–2177. doi:10.1029/2019je006054

McCoy, J. E. (1976). Photometric studies of light scattering above the lunar terminator from apollo solar corona photography. *Lunar Planet. Sci. Conf. Proc.* 7, 1087–1112.

Němeček, Z., Pavlů, J., Šafránková, J., Beránek, M., Richterová, I., Vaverka, J., et al. (2011). Lunar dust grain charging by electron impact: Dependence of the surface potential on the grain size. *Astrophysical J.* 738, 14. doi:10.1088/0004-637x/738/1/14

Örger, N. C., Toyoda, K., Masui, H., and Cho, M. (2021). Experimental investigation on particle size and launch angle distribution of lofted dust particles by electrostatic forces. *Adv. Space Res.* 68, 1568–1581. doi:10.1016/j.asr.2021.03.037

Örger, N. C., Toyoda, K., Masui, H., and Cho, M. (2019). Experimental investigation on silica dust lofting due to charging within micro-cavities and surface electric field in the vacuum chamber. *Adv. Space Res.* 63, 3270–3288. doi:10.1016/j.asr.2019.01.045

Rennilson, J., and Criswell, D. R. (1974). Surveyor observations of lunar horizon-glow. *moon* 10, 121–142. doi:10.1007/bf00655715

Schwan, J., Wang, X., Hsu, H.-W., Grün, E., and Horányi, M. (2017). The charge state of electrostatically transported dust on regolith surfaces. *Geophys. Res. Lett.* 44, 3059–3065. doi:10.1002/2017gl072909

Walton, O. R. (2007). *Adhesion of lunar dust. NASA contractor report NASA/CR-2007-214685*.

Wang, X., Horányi, M., and Robertson, S. (2011). Dust transport near electron beam impact and shadow boundaries. *Planet. Space Sci.* 59, 1791–1794. doi:10.1016/j.pss.2010.12.005

Wang, X., Horányi, M., and Robertson, S. (2010). Investigation of dust transport on the lunar surface in a laboratory plasma with an electron beam. *J. Geophys. Res. Space Phys.* 115. doi:10.1029/2010ja015465

Wang, X., Schwan, J., Hsu, H.-W., Grün, E., and Horányi, M. (2016). Dust charging and transport on airless planetary bodies. *Geophys. Res. Lett.* 43, 6103–6110. doi:10.1002/2016gl069491

Xie, L., Zhang, X., Li, L., Zhou, B., Zhang, Y., Yan, Q., et al. (2020). Lunar dust fountain observed near twilight craters. *Geophys. Res. Lett.* 47, e2020GL089593. doi:10.1029/2020gl089593

Yan, Q., Zhang, X., Xie, L., Guo, D., Li, Y., Xu, Y., et al. (2019). Weak dust activity near a geologically young surface revealed by chang'e-3 mission. *Geophys. Res. Lett.* 46, 9405–9413. doi:10.1029/2019gl083611

Zakharov, A., Zelenyi, L., and Popel', S. (2020). Lunar dust: Properties and potential hazards. *Sol. Syst. Res.* 54, 455–476. doi:10.1134/s0038094620060076

Zhang, H., Wang, Y., Chen, L., Zhang, H., Li, C., Zhuang, J., et al. (2020). *In-situ* lunar dust deposition amount induced by lander landing in chang'e-3 mission. *Sci. China Technol. Sci.* 63, 520–527. doi:10.1007/s11431-019-1434-y

Zook, H. A., and McCoy, J. E. (1991). Large scale lunar horizon glow and a high altitude lunar dust exosphere. *Geophys. Res. Lett.* 18, 2117–2120. doi:10.1029/91gl02235